Methanol on the rocks: green rust transformation promotes the oxidation of methane

Orion Farr, Nil Gaudu, Gregoire Danger, Michael Russell, Daniel Ferry, Wolfgang Nitschke, Simon Duval

Methanol on the rocks: Green rust transformation promotes the oxidation of methane

Orion Farr[a,b], Nil Gaudu[b], Gregoire Danger[c], Michael J. Russell[d], Daniel Ferry[a], Wolfgang Nitschke[b], Simon Duval[b]

a. Aix-Marseille Univ, CNRS, CINaM, F-13009, Marseille, France
b. CNRS, BIP (UMR 7281), Aix Marseille Univ, Marseille, France
c. Aix-Marseille Univ, CNRS, PiiM, F-13013, Marseille, France
d. Dipartimento di Chimica, Università degli Studi di Torino, Italy

*Corresponding author: Orion Farr

Email: orionfarr@gmail.com

I. Abstract:

Shared coordination geometries between metal ions within reactive minerals and enzymatic metal cofactors hints at mechanistic and possibly evolutionary homology between particular abiotic chemical mineralogies and biological metabolism. The octahedral coordination of reactive $Fe^{2+/3+}$ minerals such as green rusts, endemic to anoxic sediments and the early Earth's oceans, mirrors the di-iron reaction center of soluble methane monooxygenase (sMMO), responsible for methane oxidation in methanotrophy. We show that methane oxidation occurs in tandem with the oxidation of green rust to lepidocrocite and magnetite, mimicking radical mediated methane oxidation found in sMMO to yield not only methanol but also halogenated hydrocarbons in the presence of seawater. This naturally occurring geochemical pathway for CH_4 oxidation elucidates a previously unidentified carbon cycling mechanism in modern and ancient environments and reveals clues into mineral-mediated reactions in the synthesis of organic compounds necessary for the emergence of life.

II. Introduction:

Methane (CH_4), although currently present at only 1.9 ppm, is the major heat-trapping greenhouse gas in terms of its radiative forcing effect, having 80x the effect of CO_2 [1]. Anthropogenic emissions of CH_4 now outweigh natural sources produced via biotic (organic degradation) and abiotic (serpentinization, mantle degassing) mechanisms. Natural sinks exist for CH_4 but are insufficient to offset growing anthropogenic output. In the biosphere, CH_4 is readily oxidized by methanotrophs, yielding methanol (MeOH), a key metabolic intermediate towards biomass formation [2,3]. In many species this metabolism employs the enzyme soluble methane monooxygenase (sMMO) to react CH_4 with oxygen (O_2), N_2O, or H_2O_2 over an ephemeral di-Fe(IV) intermediate reaction center to achieve the conversion of CH_4 to MeOH [4]. A similar reaction mechanism takes place within man-made catalysts where Fe(IV) reaction centers embedded within mineral scaffolds are used to convert CH_4 to value-added products [5–7]. The oxidation state

Fe(IV), which is only ephemeral in nature, is crucial to the energetically demanding partial oxidation of CH_4 for biological and industrial purposes [7,8].

Methane is thought to have had an even larger role in climate regulation during the Hadean-Archean Eons 4.4 to 3.2 Ga, where the estimated atmospheric abundance of greenhouse gasses like CH_4, CO_2, and N_2O were orders of magnitude greater than modern, supplying ample CH_4 for the proliferation of primitive methanotrophs [9,10]. This anerobic metabolism, along with various others, dominated the biosphere until the emergence of oxygenic photosynthesis during the great oxidation event (GOE) [11].

Of pertinence to the experiments and outcomes reported herein, the octahedral di-iron reaction center structure of sMMO shares similar coordination geometry to the octahedral di-valent iron lattice coordination in green rusts (GR) (Figure 1) [12]. This group of naturally forming, metastable, reactive, layered double hydroxide (LDH) minerals are known for their redox capabilities in carrying out the reduction of metals (e.g., Cu, As, U), inorganic compounds (e.g., NO_3^-, ClO_4^-), and organic compounds (e.g., CT, TCE, TCM [13–18]. GR's unique structure consists of a charged octahedrally coordinated bilayer of divalent $Fe^{2+/3+}$ cations which can integrate other transition metals (e.g., Ni, Co, Zn, Mg, Al) and sandwich interchangeable anions (e.g., CO_3^{2-}, $HCOO^-$, Cl^-, SO_4^{2-}) [19]. The mineral reacts with oxygen, radicals, and temperature to undergo pH- and redox-dependent transformations into other reactive minerals, namely magnetite and lepidocrocite, playing a yet unquantified role in the geochemical cycling of sub-oxic subsurface environments [20–22]. Of note is its proposed role in marine nutrient and metal geochemical cycling prior to the GOE at ~ 2.5Ga [23,24], and its hypothesized suitability as an "abiotic enzyme" linking geochemical proto-metabolism with the evolution of enzymatic biochemistry prior to the emergence of life [12,25–27].

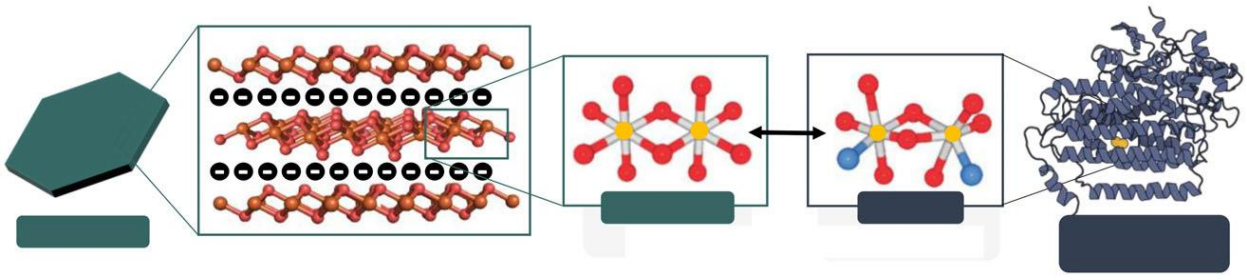

Figure 1. A diagram comparing the structural similarities between GR and sMMO. From left to right, an illustration of a single GR crystal, the crystal's cation and anion LDH structure, the octahedral coordination of iron (yellow) and oxygen (red) atoms in GR, the analogous atomic structure of the MMO reaction center (nitrogen = blue), and a model of the enzyme MMO.

The di-iron structure present in sMMO and synthetic catalysts is known to be the key site essential in the oxidation of methane. Thus, the presence of an analogous structure in GR suggests that it also has the potential to catalyze methane oxidation. In this study, we experimentally demonstrate the viability of this proposed analogous catalytic behavior by reacting green rust with CH_4 and O_2 to produce significant

quantities of MeOH and halogenated organics. These results uncover previously unrecognized redox reactions with GR and the carbon cycle, yielding significant environmental implications to the modern and ancient Earth.

III. Methods:

1.1 Mineral synthesis

Three GR species and their transformation products were synthesized following a procedure based on $GRCO_3$ syntheses outlined in Ruby (2003) and Bocher (2004). The main species of GR studied was a green rust intercalated with the carbonate anion ($GRCO_3$) and its synthesis is described below. Synthesis for $GRSO_4$ and GRCl is detailed in the supplementary section S1.

A concentrated stock solution of simulated seawater (80 ml) containing 150 mM $FeCl_2 \cdot H_2O$, 50 mM $FeCl_3$, 50 mM of MgCl, and 400 mM of NaCl was prepared using deoxygenated ultra-purified water (milli-Q) and purged with N_2 gas for 30 minutes in a sealed 125 mL reactor vial. A solution (20 ml) of 300 mM NaOH and 30 mM Na_2CO_3 was then injected into the reactor via a N_2-purged needle syringe and the mixture was gently shaken. A dark green precipitate formed which was then confirmed to be $GRCO_3$ via powder X-ray diffraction (section d), which was stable indefinitely. The total Fe concentration in this stock solution was 200 mM and final pH was ~7.

1.2 Methane oxidation reactions

The pressurized reactions took place inside a 200 ml Parr autoclave reactor pressurized to 0, 1, 10, 30, 50 bar CH_4 (Linde Gas 99.99%), 0-3 bar O_2 (Linde), 1 bar NO (Linde Gas 5%), at 25°C. Within the reactor 20-100 ml glass vials with stirrers, butyl or screw top caps, and needle-perforated septa were used to contain the replicate mineral suspensions. These vials were then removed and stored under anoxic conditions before their headspaces were analyzed using GC-MS.

1.3 Headspace Analysis

GC gas chromatography coupled to an ISQ mass spectrometer (ThermoFisher Scientific). The sampling was performed by headspace (HS) using an RSH auto-sampler (ThermoFisher Scientific). 5 mL of each sample was deposited on a 20 mL HS vial with screwtop PTFE septas. Each vial was then incubated during 6 min at 55°C under agitation. The HS sampling was performed by collecting 2 mL of the gas phase. It was then injected into the GC via an injector at 250°C, a split at 10 mL/min and a column flow of 1.1 mL/min. The column was a Stabilwax-DA from Restek (length 30m, diameter 0.25 mm, film thickness 0.5µm). Analyses were performed with the temperature gradient that starts with a 1 min isotherm at 35°C and proceeds with a gradient at 25°C/min up to 220°C ending with a 2 min isotherm. The detection was performed with the MS in full scan or SIM mode using an electron impact ionization at 70eV. MS transfer line and ion source temperatures were set at 250°C. For the full scan analyses, the m/z range was 20-300 au, meanwhile for the SIM m/z 31 and 84 were isolated for MeOH and TCM identification (Figure S6).

4.4 Mineral characterization

Mineral transformation over the course of the reaction was monitored using X-ray diffraction (XRD), transmission electron microscopy (TEM), and scanning electron microscopy (SEM). Samples were centrifuged, decanted, and dried under a stream of N_2 gas. For XRD analysis glycerol was added prior to analysis to prevent oxidation and the paste was transferred into a glass ampule for XRD analysis in a Rigaku RU 200BH diffractometer with Cu anode (λ = 1.5418Å), scanning from 2 theta values of 2-80 degrees. For TEM analysis, an aliquot of dried mineral was deposited on a copper grid coated with a holey carbon film (AGAR Scientific, S147-3). Grids were then transferred to a Jeol-JEM2010 electron microscope operated at 200 kV and GR particles were observed in bright field mode. For SEM analysis, an aliquot of dried mineral was deposited on an aluminum sample holder and then transferred to a Jeol JSM-7900F electron microscope and analyzed using accelerating voltages ranging from 5 to 15 kV.

IV. Results:

The pressurization of GR with CH_4 and O_2 resulted in the production of MeOH along with various other compounds, including trichloromethane (TCM) and dichloromethane (DCM). Various conditions were tested to optimize the yield of MeOH.

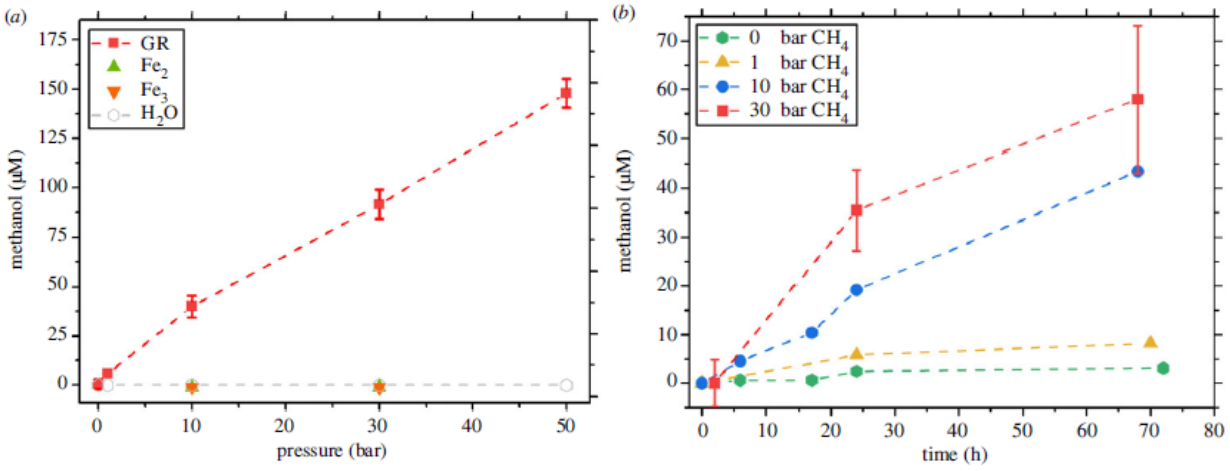

Figure 2: Effect of pressure and time on methanol concentration. (a) displays methanol concentrations at given CH_4 partial pressure following 24 hours of reaction time in solutions containing $GRCO_3$, $FeCl_2$, $FeCl_3$, and H_2O. (b) displays a related set of experiments conducted at [Fe] = 30 mM, showing methanol production over time.

Figure 2a shows MeOH concentrations in solutions of $GRCO_3$ ([Fe]=200mM) following 24 hours of pressurization to 0, 1, 10, 30, and 50 bars of CH_4 mixed with 0.2 bar O_2. There is a significant increase in

MeOH concentration with increasing pressure. At 10 bar CH_4, solutions of $GRCO_3$ with a total [Fe]= 200mM yield 30µM MeOH which increases 5-fold with a corresponding 5-fold increase to 50 bar CH_4. Thus MeOH concentration increases with a linear relationship with pressure [y =(2.88E-6)x + 5.30E-6)]. Multiple concentrations were examined and the relationship between [MeOH]/[Fe] is compared (Supplementary figure 5). MeOH is only detected with GR in the initial solution, as solutions containing $FeCl_2$, $FeCl_3$, or H_2O did not produce detectable levels of MeOH under the same conditions. No MeOH is detected without the added oxidants. Substitutes for O_2, NO and H_2O_2, were tested and found to produce products of CH_4 oxidation (Supplementary figure 7).

Figure 2b shows the production of MeOH over time in solutions of $GRCO_3$ ([Fe]=30mM) with partial pressures of CH_4 from 0 to 30 bar mixed with 0.2 bar O_2. These experiments were conducted at lower concentrations of Fe than Figure 2 (30 vs 200mM). No MeOH is detected in solutions of GR not exposed to CH_4. With 1 bar CH_4 there is a mild increase to ~5µM of MeOH. At 10 bars CH_4 there is an increase from 0 to ~40µM of MeOH by 80 hours. At 30 bar of CH_4 we show an increase from 0 to ~55µM of MeOH by 68 hours of reaction time. The addition of 0.2 bar O_2 and subsequent MeOH production resulted in changes to solution pH, which was recorded to drop from an initial value of 7 to 6 by 24 hours and 5 by ~70 hours. Additional experiments were attempted with 1 bar O_2 and 10 bar CH_4, leading to rapid mineral transformation yet no measurable MeOH production.

Coinciding with MeOH production was the production of various organic compounds produced in µM quantities. The most prevalent compounds detected other than MeOH were halogenated organics, mainly TCM and DCM (Supplementary figure 2). The concentration of TCM and DCM increased in response to increased pressure, however DCM was the primary organohalogen detected at higher pressures (30 bar) versus TCM dominating at lower pressures. Trace amounts of TCM were also detected without the presence of O_2 in aged $GRCO_3$ solutions exposed to CH_4. However, TCM was also produced in solutions of $FeCl_2$ when exposed to CH_4. Other organic products were produced but were not easily replicated and thus were not quantified: these compounds included C_1-C_{12} hydrocarbons, butanal, pentanal, paraformaldehyde, acetaldehyde, and dimethyl ether.

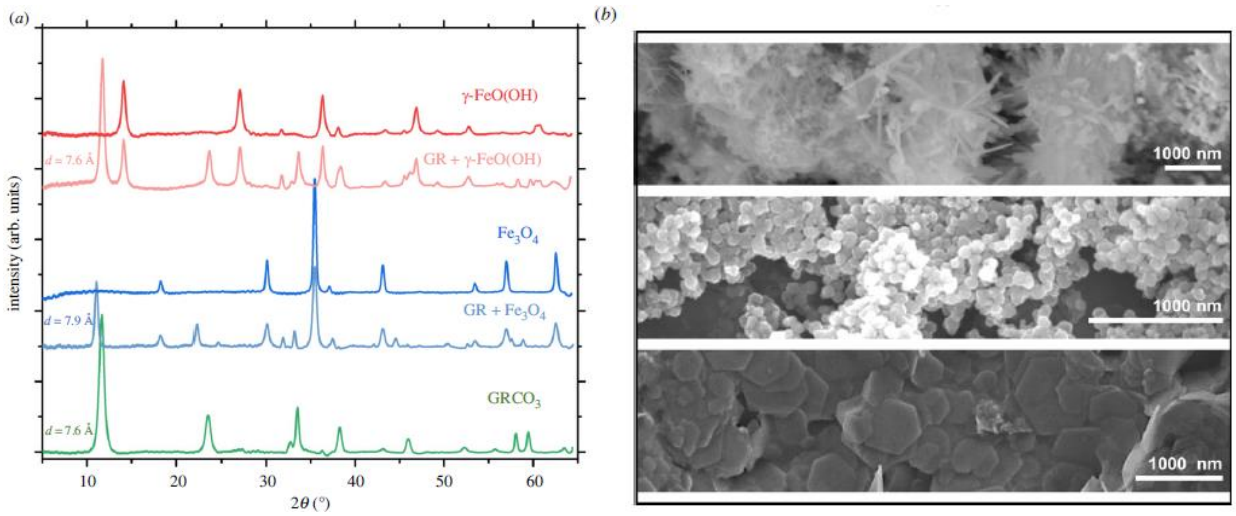

Figure 3 – Section A displays the XRD diffractograms of the mineral species produced following the exposure of GRCO3 to pressurized CH_4/O_2 atmospheres. Magnetite (Fe_3O_4) and lepidocrocite (γ-FeO(OH)) were the primary transformation products of GR corresponding to low (~0.1 bar) and high (>0.1 bar) O_2 content respectively. Partially transformed products are displayed below the primary product, with the residual GR's low 2θ d-spacing listed adjacent. Section B displays the corresponding SEM images of the pure mineral phases characterized in section A.

GR undergoes transformation to two mineral phases following the exposure to pressurized CH_4 and O_2 mixtures, oxidizing to either magnetite (Fe_3O_4) or lepidocrocite (γ-FeO(OH)) according to XRD (Figure 3a). The presence of O_2 (0-1 bar) at the start of the reaction resulted in different transformation product yields, with increased O_2 selecting for γ -FeO(OH) over Fe_3O_4. In the case of transformation to Fe_3O_4, d spacing for the low 2θ peak shifts from 7.6 A to 7.9 A. Full transformation takes place within 68 hours of reaction. SEM (Figure 3b) images show distinct transformation from GR's characteristic 10 to 500 nM hexagonal platelets, through an intermediate phase with hexagonal plates studded with <100 nM spheroid assemblages or <100nm irregular acicular crystals, to a fully transformed phase with only spheroids or acicular crystals. The transformation of GR results in a decrease from an initial average pH of 7 to 5.

v. Discussion:

Our experiments show that the oxidative transformation of GR in the presence of CH_4 results in the oxidation of CH_4, to a variety of products. In section a, we discuss the analysis of MeOH, as well as the other compounds (e.g. TCM, DCM) detected in significant quantities.

a. The concurrent oxidation of green rust and methane

The production of MeOH at various pressures and over time is depicted in figure 2, showing significant quantities are produced in solutions of GR pressurized to 1-50 bar over 60 hours, given the initial

presence of 0.2 bar of O_2 at the start of the experiment. However, in the absence of oxygen, the introduction of CH_4 to GR resulted in little to no MeOH production. Substitutes for O_2 were tested, using H_2O_2 (Supplementary figure 5) and NO (Supplementary figure 7) in separate experiments, yielding MeOH and butanal respectively. The presence of a sufficient oxidant is therefore implicated in the successful oxidation of methane using GR.

Increasing CH_4 pressure resulted in a linear increase in MeOH concentration over a range of [Fe] (200, 100, 30 mM). Increasing the concentration of Fe results in higher yield of MeOH, however the efficiency of the production of MeOH/Fe falls dramatically (Supplementary figure 5). GR's affinity to hydrophilic O_2 and as well as radical scavenging likely dominates surface interactions versus hydrophobic gases like CH_4. The reaction rate is thus dependent on how much CH_4 is in contact with the mineral surface, which is controlled by the concentration of dissolved CH_4 in solution (Figure 2). CH_4 solubility is controlled by pressure and chloride concentration due to CH_4's low solubility in distilled water at STP (25 C:1 bar) – solubility increases 42% from 1 to 50 bars but is decreased by 20% with the addition of 0.4 M Cl^- [30]. The solubilization of CH_4 is one route for aqueous mineral reactions, however within pore spaces common to sediments and hydrothermal systems where this reaction would occur, direct contact with trapped CH_4 bubbles would offer a more direct mineral-to-gas interface, increasing the reaction rate.

The substitution of interlayer anions is known to affect GR reactivity [31] and our investigation of Cl^-, CO_3^{2-}, and SO_4^{2-} (Supplementary figure 4) shows an unexpected trend in reactivity with CO_3^{2-}>Cl^->SO_4^{2-}. With prior work in GR, redox reactions involving the various anions show clear preference for Cl^- and SO_4^{2-} over CO_3^{2-} reactions [19]. A shift in d-spacing (Figure 3) from 7.6A to 7.9A corresponds to a shift in interlayer anion species from CO_3^{2-} to Cl^- during transformation from GR to Fe_3O_4[19]. As the $GRCO_3$ and GRCl solutions were conducted in simulated seawater, a mixed or transitory interlayer phase of CO_3^{2-}+Cl^- could conceivably be responsible for increased reactivity towards CH_4 oxidation. The increased MeOH production could also be linked to the reduction of interlayer bound CO_3^{2-} during the reaction [32].

The production of halogenated organic molecules was observed (Supplementary figure 2): GR appears to catalyze CH_4 chlorination as TCM and DCM are products in solutions containing GR and NaCl. GR and magnetite are known to reduce halogenated organics [33], which may explain the preference for DCM over TCM at higher pressure. Given time, this reduction should continue to methyl chloride and CH_4. Chlorine could likely be replaced by other environmentally relevant halogens such as iodine or bromine, indicating a general abiotic link between Fe redox and halogen cycling in the environment.

MeOH was not detected in parallel experiments using solutions of H_2O, NaCl, or $FeCl_2$, or $FeCl_3$ in place of GR. Since no MeOH is formed without GR or without O_2, GR must be producing a short-lived reactant during oxidation necessary for the reaction to proceed over GR or its oxide transformation products; ferric green rust, magnetite, or lepidocrocite.

b. Radicals and Fe(IV) mediated oxidation mechanism

The presence of radicals and Fe(IV) oxidation states are routinely implicated in CH_4 oxidation research as a main mechanism for achieving the energetically difficult partial oxidation of methane over transition metal bearing mineral catalysts such as zeolites [6,7]. These high surface area aluminosilicate minerals bear Fe (II-III) reaction sites which readily react with oxidative species such as O_2, H_2O_2, N_2O, UV, or radicals to create short lived reactive Fe(IV) oxidation states which can effectively conduct CH_4 oxidation [5,7,34]. This Fe(IV) state is likewise responsible for CH_4 oxidation in microbial methanotrophy, where the enzyme sMMO uses oxidant-activated Fe(IV) reaction centers to transform CH_4 to MeOH [4]. Correspondingly, in GR, it's oxidative transformation is known to produce a significant amount of hydroxyl radicals, H_2O_2, and Fe(IV) sites [35,36] which have been observed to promote the degradation of complex organic molecules [37,38].

Given the known relationship between radical production, Fe(IV) sites, and methane oxidation, we propose that GR mediates CH_4 oxidation via radical mediated oxidation pathway over short-lived Fe(IV) sites in a manner similar to sMMO [8] or Fe-ZSM zeolites [6]

To further test this hypothesis, we replicated the experimental conditions for $GRCO_3$ at 1 bar CH_4 and replaced O_2 with 1 mM of H_2O_2 which yielded a significant amount of MeOH even without high pressures (Supplementary figure 5). This indicates the reaction is dependent on the interaction between hydroxyl radicals, iron, and CH_4 [39]. Furthermore, MeOH serves as a radical scavenger resulting in its own oxidation to formaldehyde (which was detected), formate, and CO_2 [40]. The production of organohalogens in the presence of Cl^- anions, likely through a radical chlorination pathway [41], adds further evidence to the radical-based hypothesis. In this case, the Cl^- radical ion substitutes for the hydroxyl radical to oxidize CH_4 yielding methyl chloride (MC), DCM, and TCM, instead of MeOH, which was observed in our experiments.

c. Implications

The discovery of a naturally occurring mineral-based mechanism for CH_4 oxidation is novel and hints at large scale geochemical processes that have been overlooked with past research.

Feasibility and environmental relevance

The conditions simulated within the pressure reactor (GR in contact with pressurized CH_4) provided optimal conditions for the reaction in addition to serving as an analogue to environmental conditions where GR could conceivably interact with sources of CH_4 at depth. GR has been isolated in deep anoxic ferruginous lakes [21] and is speculated to form at hydrothermal vents and [42] where oxygen-poor hydrothermal fluids meet cold oxygen-rich sea water. In both locales, abiotic and biotic sources of CH_4, pressurized at depths (e.g. 100 m depth = 10 bar pressure) would fall within the range of conditions we tested. For environments closer to STP, such as wetland sediments, soils, and ground water, our

experimental results still demonstrate GR's reactivity towards CH_4 oxidation, albeit one accelerated by pressure. We observed both MeOH and halogenated organics at 1 bar CH_4, though in low concentrations, indicating that mineral based CH_4 oxidation will take place even under STP. The discovery of naturally occurring mineral-based mechanism for CH_4 oxidation is novel and hints at global geochemical processes that have been previously overlooked.

Implied role of green rust in carbon and halogen cycling in modern environments

Green rusts are well studied for their use in the degradation of organohalogen pollutants in the environment [43–46], however they have never been linked to organohalogen formation via CH_4 oxidation. Recent observations revealed that salt plains, rainforests, and soils are the source of abiotic emissions of chloromethanes [47–51]. Of note is the isotopic fractionation of some of these signatures, implying an abiotic source [50]. As mentioned previously, GR is common in these types of waterlogged environments [52] and within anoxic regions of stratified bodies of water and rivers with high iron content [21,53]. In soils, Fe is already known to halogenate decaying organic matter[47], the direct oxidation of CH_4 has not yet been observed in the environment. Our experiments show that it is feasible for GR to be oxidatively transformed to reactive Fe-oxides in the presence of CH_4, thus catalyzing abiotic CH_4 oxidation and chloromethane production. As CH_4, halomethane, and halogen flux greatly affect climate forcing [54] uncovering the role reactive minerals play in these cycles may help constrain their input over climate change. Overall, the further study of these environments should take care to identify O_2-sensitive minerals like GR, to understand the extent of their influence over the geochemical cycling of carbon and halogens.

Methane oxidation on the ancient Earth

Abiotic CH_4 oxidation may have played a greater role in the deep past as long periods of ferruginous oceans characterized the Archean (4-3.5 Ga) and Proterozoic (3.5-2 Ga) eons [24,55,56]. During these periods GRs are thought to have been abundant and likely shepherded marine geochemistry at the interface between land, air, and sea [21,24,57]. Prior to the GOE and the subsequent proliferation of O_2 in marine environments; geochemically generated radical species [39,58–61], thermochemical processes [22,62], natural electrochemical processes [63–65], photochemistry [23,61], nitrogen oxides [18,66], and nitrogen oxyanions [67,68], may have served as potential surrogates for the oxidation of GR and thus CH_4, creating a CH_4 sink within the ancient Archean ocean. As O_2 concentrations increased following the GOE, the oxidation of GR-bearing oceans may have played a role in the drawdown of atmospheric CH_4 concentrations [10], impacting climate throughout the Proterozoic [69,70].

As halomethanes exert strong influences over the greenhouse effect [54], the effect of their production by a GR saturated ocean on the Archean climate is currently unstudied. As such, the detection of exoplanet halomethane signatures may not necessarily indicate the presence of life, as was recently suggested [71]. However, as life is thought to have emerged sometime in the late Hadean to early-Archean, the oxidation of abundant CH_4 [10] to more biochemically accessible compounds such as MeOH,

hydrocarbons, and halogenated organics may have played important roles both before and after its emergence.

More specifically, our results strengthen an emergence-of-life hypothesis that invokes a pathway for GR-mediated protocell synthesis [3,12,25,26], where hydrothermal CH_4 is oxidized to multi-carbon compounds within GR-saturated mineral membranes precipitated at the redox boundary between reducing alkaline vent effluent and oxidizing acidic ocean water – the type of disequilibria considered to have driven life into being [72]. Just as in the biological metabolism of methanotrophy, methane would thereby serve both as a feedstock for production of organics and as a source of a cascade of increasingly reducing electrons derived from the further oxidation of MeOH, formaldehyde etc, as discussed in [3,63]. As pointed out previously, such entropy-decreasing processes are prerequisites for thermodynamically meaningful emergence-of-life scenarios [73]. Given the similarities between sMMO's di-iron reaction center and GR's atomic lattice coordination, a proposed evolutionary link between minerals and enzymes is suggested [74]. Because GR has a uniquely versatile structure which allows for chemical exchange; integrating several essential metals (e.g., Co, Ni, Zn, Mo) and anionic (e.g., NO^{3-}, formate, linear carbon chain) species, it is suggested that its reactive surfaces and bilaterally active interlayers served as sites for organic synthesis and concentration [75] at early submarine alkaline hydrothermal vents, and that these interlayers also compartmentalized and guided the free-energy converting proto-metabolic processes which led to the emergence of life [12,25,26].

vi. Conclusion:

We demonstrate that the oxidative transformation of green rust in the presence of methane yields methanol, along with organohalogens and various other organic compounds. This newly discovered behavior implies the existence of previously undetected links between iron, carbon, and halogen redox cycling in modern and ancient environments mediated by reactive minerals. Furthermore, the oxidation of CH_4 mediated by an abiotic GR mineral invites further research into the relationship between the evolution of primitive microbial metabolisms and the abiotic geochemical processes that preceded them.

vii. Acknowledgements:

This work received support from the French Government under the France 2030 investment plan, as part of the initiative d'Excellence d'Aix Marseille Université (A*MIDEX -AMX-21-PEP-039) as well as a grant from the French Agence Nationale pour la Recherche (ANR-22-CE30-0035-01).

We thank Vasile Heresanu for performing XRD measurements, Alexandre Altié and Damien Chaudanson for SEM/TEM support, Frederic Brunel for lending us the pressure reactor, and Olivier Grauby for helpful discussions on green rust.

viii. Authors contributions

OF designed and performed experiments. OF, NG, GD, MR, DF, WN, SD contributed to the manuscript.

ix. Conflict of interest

The authors note no conflict of interest.

x. References:

1. Jackson RB *et al.* 2021 Atmospheric methane removal: A research agenda. *Philosophical Transactions of the Royal Society A: Mathematical, Physical and Engineering Sciences* **379**. (doi:10.1098/rsta.2020.0454)

2. Chistoserdova L, Vorholt JA, Thauer RK, Lidstrom ME. 1998 C1 Transfer Enzymes and Coenzymes Linking Methylotrophic Bacteria and Methanogenic Archaea. *Science (1979)* **281**, 99–102. (doi:10.1126/science.281.5373.99)

3. Russell MJ, Nitschke W. 2017 Methane: Fuel or Exhaust at the Emergence of Life? *Astrobiology* **17**, 1053–1066. (doi:10.1089/ast.2016.1599)

4. Kopp DA, Lippard SJ. 2002 Soluble methane monooxygenase: activation of dioxygen and methane. *Curr Opin Chem Biol* **6**, 568–576. (doi:10.1016/S1367-5931(02)00366-6)

5. Nizova G V., Süss-Fink G, Shul'pin GB. 1997 Catalytic oxidation of methane to methyl hydroperoxide and other oxygenates under mild conditions. *Chemical Communications* , 397–398. (doi:10.1039/a607765j)

6. Starokon E V., Parfenov M V., Arzumanov SS, Pirutko L V., Stepanov AG, Panov GI. 2013 Oxidation of methane to methanol on the surface of FeZSM-5 zeolite. *J Catal* **300**, 47–54. (doi:10.1016/j.jcat.2012.12.030)

7. Dummer NF *et al.* 2023 Methane Oxidation to Methanol. *Chem Rev* **123**, 6359–6411. (doi:10.1021/acs.chemrev.2c00439)

8. Banerjee R, Proshlyakov Y, Lipscomb JD, Proshlyakov DA. 2015 Structure of the key species in the enzymatic oxidation of methane to methanol. *Nature* **518**, 431–434. (doi:10.1038/nature14160)

9. Arney G, Domagal-Goldman SD, Meadows VS, Wolf ET, Schwieterman E, Charnay B, Claire M, Hébrard E, Trainer MG. 2016 The Pale Orange Dot: The Spectrum and Habitability of Hazy Archean Earth. *Astrobiology* **16**, 873–899. (doi:10.1089/ast.2015.1422)

10. Catling DC, Zahnle KJ. 2020 The Archean atmosphere. *Sci Adv* **6**. (doi:10.1126/sciadv.aax1420)

11. Schirrmeister BE, Gugger M, Donoghue PCJ. 2015 Cyanobacteria and the Great Oxidation Event: Evidence from genes and fossils. *Palaeontology* **58**, 769–785. (doi:10.1111/pala.12178)

12. Duval S, Baymann F, Schoepp-Cothenet B, Trolard F, Bourrié G, Grauby O, Branscomb E, Russell MJ, Nitschke W. 2019 Fougerite: The not so simple progenitor of the first cells. *Interface Focus* **9**, 16–20. (doi:10.1098/rsfs.2019.0063)

13. Jönsson J, Sherman DM. 2008 Sorption of As(III) and As(V) to siderite, green rust (fougerite) and magnetite: Implications for arsenic release in anoxic groundwaters. *Chem Geol* **255**, 173–181. (doi:10.1016/j.chemgeo.2008.06.036)

14. Døssing LN, Dideriksen K, Stipp SLS, Frei R. 2011 Reduction of hexavalent chromium by ferrous iron: A process of chromium isotope fractionation and its relevance to natural environments. *Chem Geol* **285**, 157–166. (doi:10.1016/j.chemgeo.2011.04.005)

15. Choi J, Batchelor B, Won C, Chung J. 2012 Nitrate reduction by green rusts modified with trace metals. *Chemosphere* **86**, 860–865. (doi:10.1016/j.chemosphere.2011.11.035)

16. Etique M, Zegeye A, Grégoire B, Carteret C, Ruby C. 2014 Nitrate reduction by mixed iron(II-III) hydroxycarbonate green rust in the presence of phosphate anions: The key parameters influencing the ammonium selectivity. *Water Res* **62**, 29–39. (doi:10.1016/j.watres.2014.05.028)

17. Onoguchi A, Granata G, Haraguchi D, Hayashi H, Tokoro C. 2019 Kinetics and mechanism of selenate and selenite removal in solution by green rust-sulfate. *R Soc Open Sci* **6**. (doi:10.1098/rsos.182147)

18. Buessecker S, Imanaka H, Ely T, Hu R, Romaniello SJ, Cadillo-Quiroz H. 2022 Mineral-catalysed formation of marine NO and N2O on the anoxic early Earth. *Nat Geosci* **15**, 1056–1063. (doi:10.1038/s41561-022-01089-9)

19. Usman M, Byrne JM, Chaudhary A, Orsetti S, Hanna K, Ruby C, Kappler A, Haderlein SB. 2018 Magnetite and Green Rust: Synthesis, Properties, and Environmental Applications of Mixed-Valent Iron Minerals. *Chem Rev* **118**, 3251–3304. (doi:10.1021/acs.chemrev.7b00224)

20. Trolard F, Bourrié G. 2008 *Chapter 5 Geochemistry of Green Rusts and Fougerite. A Reevaluation of Fe cycle in Soils*. (doi:10.1016/S0065-2113(08)00405-7)

21. Zegeye A *et al.* 2012 Green rust formation controls nutrient availability in a ferruginous water column. *Geology* **40**, 599–602. (doi:10.1130/G32959.1)

22. Farr O, Elzinga EJ, Yee N. 2022 Effect of Ni2+, Zn2+, and Co2+ on green rust transformation to magnetite. *Geochem Trans* **23**, 3. (doi:10.1186/s12932-022-00080-y)

23. Dodd MS *et al.* 2022 Abiotic anoxic iron oxidation, formation of Archean banded iron formations, and the oxidation of early Earth. *Earth Planet Sci Lett* **584**. (doi:10.1016/j.epsl.2022.117469)

24. Halevy I, Alesker M, Schuster EM, Popovitz-Biro R, Feldman Y. 2017 A key role for green rust in the Precambrian oceans and the genesis of iron formations. *Nat Geosci* **10**, 135–139. (doi:10.1038/ngeo2878)

25. Russell M. 2018 Green Rust: The Simple Organizing ‘Seed’ of All Life? *Life* **8**, 35. (doi:10.3390/life8030035)

26. Russell MJ. 2023 A self-sustaining serpentinization mega-engine feeds the fougerite nanoengines implicated in the emergence of guided metabolism. *Front Microbiol* **14**. (doi:10.3389/fmicb.2023.1145915)

27. Barge LM, Flores E, Baum MM, Velde DGV, Russell MJ. 2019 Redox and pH gradients drive amino acid synthesis in iron oxyhydroxide mineral systems. *Proc Natl Acad Sci U S A* **116**, 4828–4833. (doi:10.1073/pnas.1812098116)

28. Ruby C, Géhin A, Abdelmoula M, Génin JMR, Jolivet JP. 2003 Coprecipitation of Fe(II) and Fe(III) cations in sulphated aqueous medium and formation of hydroxysulphate green rust. *Solid State Sci* **5**, 1055–1062. (doi:10.1016/S1293-2558(03)00121-3)

29. Bocher F, Géhin A, Ruby C, Ghanbaja J, Abdelmoula M, Génin JMR. 2004 Coprecipitation of Fe(II-III) hydroxycarbonate green rust stabilised by phosphate adsorption. *Solid State Sci* **6**, 117–124. (doi:10.1016/j.solidstatesciences.2003.10.004)

30. Duan Z, Møller N, Greenberg J, Weare JH. 1992 The prediction of methane solubility in natural waters to high ionic strength from 0 to 250°C and from 0 to 1600 bar. *Geochim Cosmochim Acta* **56**, 1451–1460. (doi:10.1016/0016-7037(92)90215-5)

31. Agnel MI, Grangeon S, Fauth F, Elkaïm E, Claret F, Roulet M, Warmont F, Tournassat C. 2020 Mechanistic and Thermodynamic Insights into Anion Exchange by Green Rust. *Environ Sci Technol* **54**, 851–861. (doi:10.1021/acs.est.9b05632)

32. Lee S, Wang C, Chakrapani V. In press. Spontaneous Unassisted Conversion of CO 2 to Multicarbon Liquid Products on Green Rust Mineral. (doi:10.26434/chemrxiv-2023-bch3f-v2)

33. Erbs M, Hansen HCB, Olsen CE. 1999 Reductive dechlorination of carbon tetrachloride using iron(II) iron(III) hydroxide sulfate (green rust). *Environ Sci Technol* **33**, 307–311. (doi:10.1021/es980221t)

34. Szécsényi Á, Li G, Gascon J, Pidko EA. 2018 Mechanistic Complexity of Methane Oxidation with H2O2 by Single-Site Fe/ZSM-5 Catalyst. *ACS Catal* **8**, 7961–7972. (doi:10.1021/acscatal.8b01672)

35. Fang L, Xu L, Deng J, Gao S, Huang LZ. 2021 Induced generation of hydroxyl radicals from green rust under oxic conditions by iron-phosphate complexes. *Chemical Engineering Journal* **414**, 128780. (doi:10.1016/j.cej.2021.128780)

36. Li Z, Li M, Tan B, Du N, Zhang Q, Li C, Zhang Y, Li J, Li J. 2022 Green rust (GR) and glucose oxidase (GOX) based Fenton-like reaction: Capacity of sustainable release, promoted conversion of glucose through GOX-iron and pH self-adjustment. *Environ Res* **208**. (doi:10.1016/j.envres.2021.112656)

37. Hanna K, Kone T, Ruby C. 2010 Fenton-like oxidation and mineralization of phenol using synthetic Fe(II)-Fe(III) green rusts. *Environmental Science and Pollution Research* **17**, 124–134. (doi:10.1007/s11356-009-0148-y)

38. Matta R, Hanna K, Chiron S. 2008 Oxidation of phenol by green rust and hydrogen peroxide at neutral pH. *Sep Purif Technol* **61**, 442–446. (doi:10.1016/j.seppur.2007.12.005)

39. Anipsitakis GP, Dionysiou DD. 2004 Radical Generation by the Interaction of Transition Metals with Common Oxidants. *Environ Sci Technol* **38**, 3705–3712. (doi:10.1021/es035121o)

40. Alshehri A. 2013 Methanol oxidation on transition elements oxides. *PhD Thesis - Cardiff University*

41. Rabiu AM, Yusuf IM. 2013 Industrial Feasiblity of Direct Methane Conversion to Hydrocarbons over Fe-Based Fischer Tropsch Catalyst. *Journal of Power and Energy Engineering* **01**, 41–46. (doi:10.4236/jpee.2013.15006)

42. Trolard F, Duval S, Nitschke W, Ménez B, Pisapia C, Ben Nacib J, Andréani M, Bourrié G. 2022 Mineralogy, geochemistry and occurrences of fougerite in a modern hydrothermal system and its implications for the origin of life. *Earth Sci Rev* **225**. (doi:10.1016/j.earscirev.2021.103910)

43. Maithreepala RA, Doong RA. 2005 Enhanced dechlorination of chlorinated methanes and ethenes by chloride green rust in the presence of copper(II). *Environ Sci Technol* **39**, 4082–4090. (doi:10.1021/es048428b)

44. Choi J, Lee W. 2008 Enhanced degradation of tetrachloroethylene by green rusts with platinum. *Environ Sci Technol* **42**, 3356–3362. (doi:10.1021/es702661d)

45. O'Loughlin EJ, Burris DR. 2022 Reduction of Chlorinated Ethenes by Ag- and Cu-Amended Green Rust. *Minerals* **12**, 138. (doi:10.3390/min12020138)

46. Yao W, Zhang J, Gu K, Li J, Qian J. 2022 Synthesis, characterization and performances of green rusts for water decontamination: A review. *Environmental Pollution*. **304**. (doi:10.1016/j.envpol.2022.119205)

47. Huber SG, Kotte K, Schöler HF, Williams J. 2009 Natural abiotic formation of trihalomethanes in soil: Results from laboratory studies and field samples. *Environ Sci Technol* **43**, 4934–4939. (doi:10.1021/es8032605)

48. Redeker KR, Kalin RM. 2012 Methyl chloride isotopic signatures from Irish forest soils and a comparison between abiotic and biogenic methyl halide soil fluxes. *Glob Chang Biol* **18**, 1453–1467. (doi:10.1111/j.1365-2486.2011.02600.x)

49. Wittmer J, Bleicher S, Ofner J, Zetzsch C. 2015 Iron(III)-induced activation of chloride from artificial sea-salt aerosol. *Environmental Chemistry* **12**, 461–475. (doi:10.1071/EN14279)

50. Bahlmann E, Keppler F, Wittmer J, Greule M, Schöler HF, Seifert R, Zetzsch C. 2019 Evidence for a major missing source in the global chloromethane budget from stable carbon isotopes. *Atmos Chem Phys* **19**, 1703–1719. (doi:10.5194/acp-19-1703-2019)

51. Sattler T *et al.* 2019 Natural formation of chloro- and bromoacetone in salt lakes of Western Australia. *Atmosphere (Basel)* **10**. (doi:10.3390/atmos10110663)

52. Trolard F, Génin J-MR, Abdelmoula M, Bourrié G, Humbert B, Herbillon A. 1997 Identification of a green rust mineral in a reductomorphic soil by Mossbauer and Raman spectroscopies. *Geochim Cosmochim Acta* **61**, 1107–1111. (doi:10.1016/S0016-7037(96)00381-X)

53. Jorand F, Zegeye A, Ghanbaja J, Abdelmoula M. 2011 The formation of green rust induced by tropical river biofilm components. *Science of The Total Environment* **409**, 2586–2596. (doi:10.1016/j.scitotenv.2011.03.030)

54. Li Q, Fernandez RP, Hossaini R, Iglesias-Suarez F, Cuevas CA, Apel EC, Kinnison DE, Lamarque JF, Saiz-Lopez A. 2022 Reactive halogens increase the global methane lifetime and radiative forcing in the 21st century. *Nat Commun* **13**. (doi:10.1038/s41467-022-30456-8)

55. Poulton SW, Canfeld DE. 2011 Ferruginous conditions: A dominant feature of the ocean through Earth's history. *Elements* **7**, 107–112. (doi:10.2113/gselements.7.2.107)

56. Thibon F, Blichert-Toft J, Tsikos H, Foden J, Albalat E, Albarede F. 2019 Dynamics of oceanic iron prior to the Great Oxygenation Event. *Earth Planet Sci Lett* **506**, 360–370. (doi:10.1016/j.epsl.2018.11.016)

57. Koeksoy E, Sundman A, Byrne JM, Lohmayer R, Planer-Friedrich B, Halevy I, Konhauser KO, Kappler A. 2019 Formation of green rust and elemental sulfur in an analogue for oxygenated ferro-euxinic transition zones of Precambrian oceans. *Geology* **47**, 211–214. (doi:10.1130/G45501.1)

58. He H, Wu X, Xian H, Zhu J, Yang Y, Lv Y, Li Y, Konhauser KO. 2021 An abiotic source of Archean hydrogen peroxide and oxygen that pre-dates oxygenic photosynthesis. *Nat Commun* **12**. (doi:10.1038/s41467-021-26916-2)

59. Zhao G, Tan M, Wu B, Zheng X, Xiong R, Chen B, Kappler A, Chu C. 2023 Redox Oscillations Activate Thermodynamically Stable Iron Minerals for Enhanced Reactive Oxygen Species Production. *Environ Sci Technol* (doi:10.1021/acs.est.3c02302)

60. He H *et al.* 2023 A mineral-based origin of Earth's initial hydrogen peroxide and molecular oxygen. *Proc Natl Acad Sci U S A* **120**. (doi:10.1073/pnas.2221984120)

61. Ernst L, Barayeu U, Hädeler J, Dick TP, Klatt JM, Keppler F, Rebelein JG. 2023 Methane formation driven by light and heat prior to the origin of life and beyond. *Nat Commun* **14**, 4364. (doi:10.1038/s41467-023-39917-0)

62. Huang Q, Jiang S-Y, Pi D-H, Konhauser KO, Wen X-P, Lu L-Y, Yan H. 2023 Thermochemical oxidation of methane by manganese oxides in hydrothermal sediments. *Commun Earth Environ* **4**, 224. (doi:10.1038/s43247-023-00891-6)

63. Nitschke W *et al.* 2022 Aqueous electrochemistry: The toolbox for life's emergence from redox disequilibria. *Electrochemical Science Advances* (doi:10.1002/elsa.202100192)

64. Ooka H, McGlynn SE, Nakamura R. 2019 Electrochemistry at Deep-Sea Hydrothermal Vents: Utilization of the Thermodynamic Driving Force towards the Autotrophic Origin of Life. *ChemElectroChem*. **6**, 1316–1323. (doi:10.1002/celc.201801432)

65. Lee S, Wang C, Chakrapani V. 2023 Spontaneous Unassisted Conversion of CO 2 to Multicarbon (≥ C 2) Liquid Products on Green Rust Mineral. *ChemRxiv* (doi:10.26434/chemrxiv-2023-bch3f)

66. Wong ML, Charnay BD, Gao P, Yung YL, Russell MJ. 2017 Nitrogen Oxides in Early Earth's Atmosphere as Electron Acceptors for Life's Emergence. *Astrobiology* **17**, 975–983. (doi:10.1089/ast.2016.1473)

67. Ducluzeau AL, van Lis R, Duval S, Schoepp-Cothenet B, Russell MJ, Nitschke W. 2009 Was nitric oxide the first deep electron sink? *Trends Biochem Sci* **34**, 9–15. (doi:10.1016/j.tibs.2008.10.005)

68. Barge LM *et al.* 2022 Prebiotic reactions in a Mars analog iron mineral system: Effects of nitrate, nitrite, and ammonia on amino acid formation. *Geochim Cosmochim Acta* **336**, 469–479. (doi:10.1016/j.gca.2022.08.038)

69. Guilbaud R, Poulton SW, Butterfield NJ, Zhu M, Shields-Zhou GA. 2015 A global transition to ferruginous conditions in the early Neoproterozoic oceans. *Nat Geosci* **8**, 466–470. (doi:10.1038/NGEO2434)

70. Jaziri AY, Charnay B, Selsis F, Leconte J, Lefèvre F. 2022 Dynamics of the Great Oxidation Event from a 3D photochemical-climate model. *Climate of the Past* **18**, 2421–2447. (doi:10.5194/cp-18-2421-2022)

71. Leung M, Schwieterman EW, Parenteau MN, Fauchez TJ. 2022 Alternative Methylated Biosignatures. I. Methyl Bromide, a Capstone Biosignature. *Astrophys J* **938**, 6. (doi:10.3847/1538-4357/ac8799)

72. Russell MJ, Nitschke W, Branscomb E. 2013 The inevitable journey to being. *Philosophical Transactions of the Royal Society B: Biological Sciences* **368**. (doi:10.1098/rstb.2012.0254)

73. Branscomb E, Russell MJ. 2018 Frankenstein or a Submarine Alkaline Vent: Who is Responsible for Abiogenesis?: Part 2: As life is now, so it must have been in the beginning. *BioEssays*. **40**. (doi:10.1002/bies.201700182)

74. Nitschke W, McGlynn SE, Milner-White EJ, Russell MJ. 2013 On the antiquity of metalloenzymes and their substrates in bioenergetics. *Biochim Biophys Acta Bioenerg* **1827**, 871–881. (doi:10.1016/j.bbabio.2013.02.008)

75. Helmbrecht V, Weingart M, Klein F, Braun D, Orsi WD. 2022 White and green rust chimneys accumulate RNA in a ferruginous chemical garden. *ArXiv* , 1–25. (doi:10.48550/arXiv.2212.02793)